Single Scanner BLS System for Forest Plot Mapping

Jie Shao, Wuming Zhang, Nicolas Mellado, Shuangna Jin, Shangshu Cai, Lei Luo, Lingbo Yang, Guangjian Yan, *Senior Member, IEEE*, and Guoqing Zhou

***Abstract*— The 3-D information collected from sample plots is significant for forest inventories. Terrestrial laser scanning (TLS) has been demonstrated to be an effective device in data acquisition of forest plots. Although TLS is able to achieve precise measurements, multiple scans are usually necessary to collect more detailed data, which generally requires more time in scan preparation and field data acquisition. In contrast, mobile laser scanning (MLS) is being increasingly utilized in mapping due to its mobility. However, the geometrical peculiarity of forests introduces challenges. In this article, a test backpack-based MLS system, i.e., backpack laser scanning (BLS), is designed for forest plot mapping without a global navigation satellite system/inertial measurement unit (GNSS-IMU) system. To achieve accurate matching, this article proposes to combine the line and point features for calculating transformation, in which the line feature is derived from trunk skeletons. Then, a scan-to-map matching strategy is proposed for correcting positional drift. Finally, this article evaluates the effectiveness and the mapping accuracy of the proposed method in forest sample plots. The experimental results indicate that the proposed method achieves accurate forest plot mapping using the BLS; meanwhile, compared to the existing methods, the proposed method utilizes the geometric attributes of the trees and reaches a lower mapping error, in which the mean errors and the root square mean errors for the horizontal/vertical direction in plots are less than 3 cm.**

***Index Terms*— Backpack laser scanning (BLS), forest plot, mobile mapping, point cloud, simultaneous localization, and mapping (SLAM).**

Manuscript received November 5, 2019; revised March 16, 2020 and April 19, 2020; accepted May 22, 2020. This work was supported in part by the National Natural Science Foundation of China under Grant 41671414 and Grant 41971380, in part by the Guangxi Natural Science Fund for Innovation Research Team under Grant 2019JJF50001, and in part by the Open Fund of State Key Laboratory of Remote Sensing Science under Grant OFSLRSS201920. *(Corresponding author: Wuming Zhang.)*

Jie Shao is with the State Key Laboratory of Remote Sensing Science, Beijing Engineering Research Center for Global Land Remote Sensing Products, Institute of Remote Sensing Science and Engineering, Faculty of Geographical Science, Beijing Normal University, Beijing 100875, China, and also with IRIT, CNRS, University of Toulouse, 31062 Toulouse, France (e-mail: shaojie@mail.bnu.edu.cn).

Wuming Zhang is with the School of Geospatial Engineering and Science, Sun Yat-sen University, Zhuhai 519082, China, and also with Southern Marine Science and Engineering Guangdong Laboratory (Zhuhai), Zhuhai 519082, China (e-mail: zhangwm25@mail.sysu.edu.cn).

Nicolas Mellado is with IRIT, CNRS, University of Toulouse, 31062 Toulouse, France (e-mail: nicolas.mellado@irit.fr).

Shuangna Jin, Shangshu Cai, and Guangjian Yan are with the State Key Laboratory of Remote Sensing Science, Beijing Engineering Research Center for Global Land Remote Sensing Products, Institute of Remote Sensing Science and Engineering, Faculty of Geographical Science, Beijing Normal University, Beijing 100875, China.

Lei Luo is with Aerospace Information Research Institute, Chinese Academy of Sciences, Beijing 100094, China.

Lingbo Yang is with the College of Environment and Resource Sciences, Zhejiang University, Hangzhou 310058, China.

Guoqing Zhou is with the Guangxi Key Laboratory of Spatial Information and Geomatics, Guilin University of Technology, Guilin 541006, China.

Color versions of one or more of the figures in this article are available online at http://ieeexplore.ieee.org.

Digital Object Identifier 10.1109/TGRS.2020.2999413

I. Introduction

PRECISE structural information collected from field measurements is necessary for forest inventories, decision making on forest resources, and ecological studies. Most of the field measurements in a forest are based on field sample plots, and these sample plots are typically representative of the entire area of interest [1]. Generally, it is expensive to measure plots utilizing conventional and simple measurement tools. With the development of remotely sensed techniques, a frequently used method of the forest measurements is known as the light detection and ranging (LiDAR) technique, and a common method uses laser scanners [2], [3]. One of the aims of the LiDAR technique is mapping of the surrounding environment [4]. In this context, LiDAR-based mapping has become an active research topic for forest inventories.

Terrestrial laser scanning (TLS) has shown an advantage in highly accurate forest mapping [5], [6]. TLS devices use either a pulsed or continuous frequency-modulated laser beams that measure the distance to an intercepting surface and allow for the precise location of the object surface to be determined and can create a highly detailed point cloud representation of the scanning domain [7]. However, the occlusion effect limits the use of the LiDAR device in forests [8]. To tackle the occlusion effect, multiscan TLS is typically used to scan plots [9]. However, prescan preparations are generally required, e.g., placing artificial targets [10], which increases the cost of data collection, increasingly hindered by the increasing size of the forest plot to be mapped. Laser scanners have been mounted on moving platforms to build mobile laser scanning (MLS) systems and are being used for forests. Compared to the TLS system, the main advantage of MLS is the immensely rapid data collection in forest environments. Thus, it has great opportunities for increasing the cost-effectiveness of TLS [11], [12]. The greatest challenge for MLS is positional accuracy, which is closely connected with the accuracy of mapping.

Due to the ability of the global navigation satellite system (GNSS) to position the sensor and the ability of the inertial measurement unit (IMU) to produce the attitude information,

the GNSS-IMU system is usually used to derive the trajectory information of MLS for various mapping tasks [13]–[15]. The GNSS works accurately in clear sky conditions, but the task becomes increasingly difficult when satellite visibility decreases or multipath effects increase [16]. In forests, satellite availability largely depends on the amount of coverage by the canopy, and the dense canopy absorbs, reflects, or completely blocks the GNSS radio frequency signal, causing either a poor signal or signal loss. Even with a high-precision GNSS-IMU system, the positioning error can grow to several tens of centimeters and even to meters due to trajectory drift and will greatly limit the mapping accuracy in the dense forest scenes. In such cases, the scanner MLS needs to be repositioned during the mapping step, which leads to the so-called simultaneous localization and mapping (SLAM) problem [17].

SLAM is the process of mapping an unknown environment and locating the mobile platform simultaneously, which has now been widely used to provide positioning information in various environments [18]. In the initial stage of the SLAM technique, a common sensor is a camera, and currently, many excellent methods have been proposed for positioning and mapping based on the camera, e.g., monocular SLAM (MonoSLAM) [19], large-scale direct monocular SLAM (LSD-SLAM) [20], SVO: fast semidirect monocular visual odometry (SVO) [21], and ORB-SLAM: a versatile and accurate monocular SLAM system (ORB-SLAM) [22]. However, these methods require matching of landmarks and are generally limited by depth precision. By contrast, LiDAR typically has an advantage in highly precise depth measurements.

Similarly, some LiDAR-based SLAM methods have been developed for 3-D mapping of various environments, such as Hector SLAM [23], Gmapping [24], Karto-SLAM [25], and Cartographer [26]. The Hector SLAM and Gmapping methods achieved the mapping based on the filter method which relies on assumptions of the motion model and commonly has difficulty dealing with the loop-closure problem. Moreover, Karto-SLAM and Cartographer are so-called graph-based algorithms, which represent the map by means of graphs that consist of nodes and edges. In a graph, each node represents a pose of the sensor and each edge connects two successive nodes and represents the motion between the two nodes [27]. The related methods typically maintain a pose graph, that is, using only the pose information, which can suffice for the accuracy requirement of general mapping (e.g., indoor or urban mapping), but their mapping results encounter difficulty meeting the requirement of high-precision forest measurement. Additionally, some methods consider simultaneously optimizing pose and object features, which can generally achieve highly accurate mapping, such as lidar odometry and mapping in real-time (LOAM) [28] and implicit moving least squares SLAM (IMLS-SLAM) [29]. The related methods typically consist of these steps: feature extraction, matching, and mapping update. In the literature, the features, including the point, line, and plane of both the camera-based SLAM technique and the LiDAR-based SLAM technique, are usually used to estimate the position and attitude of the sensors. For example, LOAM selects the line and plane features that are extracted from the object surface, and solves the matching problem by minimizing the distances between the features and their correspondences to achieve mapping. In the feature-based SLAM method, the position and attitude solution are continuing to mature, but the feature selection limits the effectiveness of the methods in various scenes. For MLS data, the feature-based methods can acquire satisfactory solutions due to rich and clear geometrical features in indoor and urban scenes [30]. However, the features are not stable or continuous in forest environments. In addition, objects in the forests are remarkably similar and easily cause inaccurate corresponding pairs [31], [32]. Moreover, during the nonlinear optimization process, the scan matching easily falls into local minima when the scans are matched with an inaccurate initial transformation in forests. Therefore, the feature selection poses challenges to the feature-based methods in forest mapping.

Some works have presented SLAM-based mapping methods using the tree attributes and are specific to the forest scenarios. For example, Chen *et al.* [33] utilized existing map information (e.g., the center and radius of tree stems) to improve SLAM positioning in a forest. Kukko *et al.* [34] extracted the stems and correct the MLS forest data based on the graph-based SLAM. Nevertheless, these methods commonly rely on the GNSS and IMU measurements for forest mapping and may encounter the problem of the aforementioned GNSS signal blocking in dense forests. Significantly, the tree attributes (e.g., stems) have been considered for use in MLS-based forest mapping. In practice, there are many studies for registration of forest point clouds without the GNSS and IMU system and are based on natural geometrical features of trees. In the literature, the attributes of tree stems, e.g., stem curves [35] and the topological relation between the stems [32], [36], are commonly adopted to execute automated registration of forest point clouds. However, these studies mainly serve for the coregistration of dense point clouds, e.g., TLS to TLS data. In addition, these methods focus on coarse alignment of point clouds and need a fine registration in postprocessing. The iterative closest point (ICP) method [37] is now the standard approach for fine registration. It starts by searching the correspondences between point clouds and then minimizes the distance between these correspondences. Thus, the method requires a sufficient overlap of points for obtaining accurate correspondences. Nevertheless, the sparsity of single-frame MLS point cloud and the lack of overlapping points between two scans caused by different MLS scan locations easily lead to inaccurate pairs and affects registration results. Therefore, this method is ill-suited to forest scenes.

MLS-based mapping has increasingly gained attention in various scenes. However, the complex structure and irregular shape of the natural elements in the forest introduce challenges to the existing methods using an MLS device. Therefore, the authors integrate a single scanner backpack laser scanning (BLS) system without the GNSS-IMU system and propose a novel mapping method specific to forest environments. Specifically, two steps, scan-to-scan matching and scan-to-map matching, are implemented in the proposed mapping method. In the matching step, we assume that tree boles are approximately circular in cross section and extract trunk skeleton lines that represent the center lines of stems for

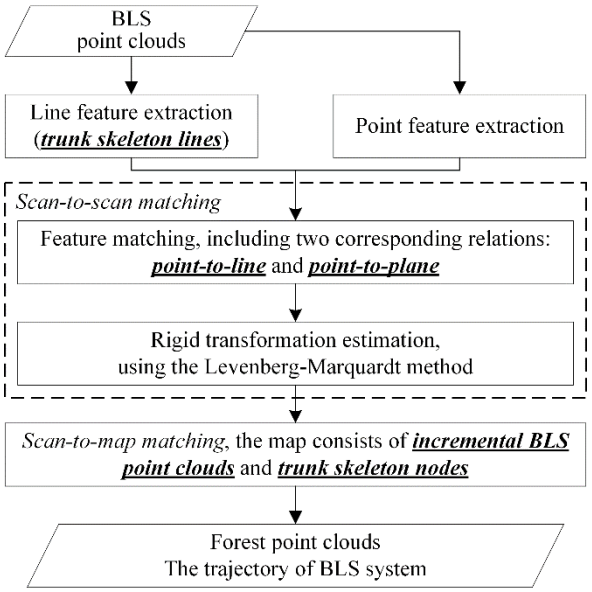

Fig. 1. Flowchart of BLS-based forest mapping.

feature matching, which can prevent inaccurate corresponding pairs and allow scan matching with low overlap. Then, all the BLS scans are mitigated of accumulative errors by performing the scan-to-map matching step, in which two maps, including the incremental BLS point clouds and trunk skeletons, are used to prevent errors after consecutive scan matchings. Following the Introduction, the overview and keys of the proposed method are elaborated in Section II. Section III introduces the performance of the proposed method. Finally, discussions and conclusions are presented.

II. Proposed Method

A. Outline of the Method

In this article, we focus our attention on forest plot mapping using a single scanner. First, a test BLS system is designed for acquisition of point clouds. Then, a SLAM-based method is implemented for forest plot mapping, which consists of three components: feature extraction, scan-to-scan matching, and scan-to-map matching. Scan-to-scan matching contains feature matching and rigid transformation estimation. In practice, we propose the combination of the semantic line and point features for scan-to-scan matching, in which the lines are derived from the tree trunk skeletons that are natural geometric elements of trees, and the points are extracted from each frame BLS point cloud evenly. Finally, we use a scan-to-map matching strategy to mitigate the accumulative errors of all the point clouds, in which the map that contains the incremental BLS point clouds and their corresponding tree trunk skeleton nodes is used to provide consistency constraints and optimize the pose of each BLS point cloud. The flowchart is shown in Fig. 1.

B. Feature Extraction

In the feature-based SLAM method, feature extraction is the precondition of localization and mapping. To achieve accurate matching, we propose to combine the line and point features to locate the scanner in this article, of which the line features are mainly used to optimize the matching error in the horizontal direction and the point features are used to ensure the vertical accuracy.

1) Line Features: For BLS data collected from different viewpoints, accurate corresponding pairs between the two frames are difficult to extract directly due to the sparsity of data and the complexity of natural elements. In the forest, tree trunks are remarkable and stable [38]. Although the surface of the tree trunks rarely has significant geometric features, the tree trunk skeletons that represent the tree center lines can provide stable and robust constraints for motion estimation of the scanner, especially in the horizontal direction. Therefore, we study a hierarchical clustering method to extract the tree trunk skeletons from each frame of the BLS point clouds.

According to the characteristics of the BLS data used, the BLS point cloud is first divided into multiple subsets based on the vertical angular resolution. This means that each subset is a full field-of-view point cloud at a fixed vertical scan angle. For each subset, distance-based region growing is used to segment objects. Initially, a random point in each subset is regarded as seed point and labeled as a new class, and the neighboring points in a specified radius of the seed point are labeled as the class of the seed, in which the radius value is set to the maximum diameter at breast height (DBH) value. If one of the neighboring points has been labeled, all the other neighboring points and the seed point are regarded as the class of the labeled point. Similarly, we traverse all the unlabeled points and determine their classes. After, we can obtain different segmentations, including the ground points, tree stem points, and canopy points, in which the segmentation that has its point number less than a set threshold will be regarded as the outlier and removed. Next, we will determine the stem points for detection of trunk skeletons. First, if the distance between the two farthest points in segmentation is out of the range of minimum DBH to maximum DBH, the segmentation will be discarded. Then, due to the characteristic of the tree, for each segmentation, the circle fit based on the weighted least-squares method [39] is used to determine the stem points. Specifically, if the diameter of a fit circle is between the minimum DBH and the maximum DBH, the corresponding segmentation will be labeled as the tree stem; meanwhile, the center points of the detected circles are regarded as trunk skeleton nodes, and the nodes that are continuously distributed in the vertical direction are considered to be derived from a trunk skeleton, in which the connected line between two neighbor nodes is regarded as a line feature (Fig. 2).

2) Point Features: The trunk skeletons contribute to reducing horizontal error of forest mapping results, but due to the approximate parallel relationship among tree trunk skeletons, the line features have difficulty providing effective constraints for feature matching in the vertical direction. Therefore, we detect some points that are evenly distributed in each frame point cloud to provide an overall constraint for the matching process. Specifically, the difference of Gaussian (DoG) approach [40] is used to extract point features. The major advantages of DoG features are their invariance to scaling,

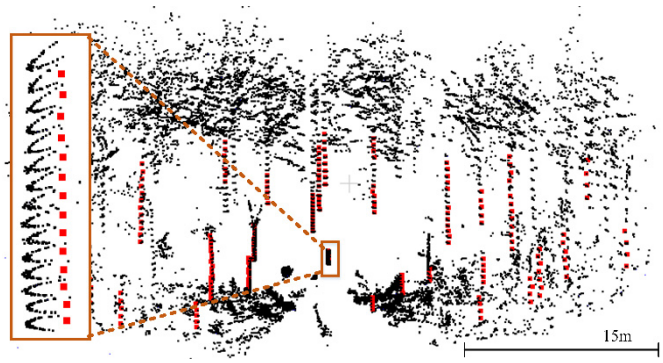

Fig. 2. Line features extraction. Extracting trunk skeleton nodes (red points), skeleton lines can be generated by connecting the neighboring nodes.

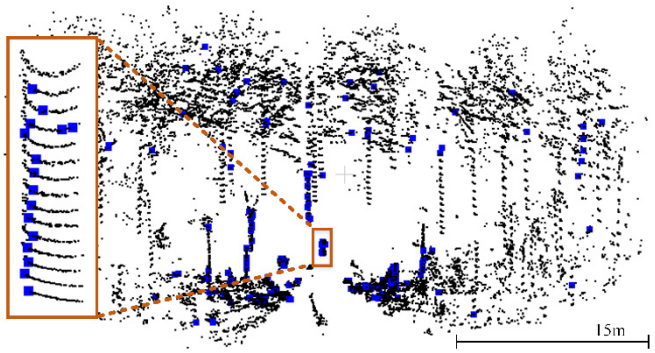

Fig. 3. Point features extraction (blue points are the extracted features).

rotation, and translation [41]. Thus, we directly extract features based on the point range.

The principle of DoG-based 3-D point feature extraction is subtracting one blurred point cloud level from another blurred level. The blurred levels are obtained by convolving the BLS point cloud with Gaussian kernels having different standard deviations (SDs). We first use the statistical outlier removal (SOR) filter to remove the outliers [42]. Next, two blurred levels of the filtered point cloud are calculated by using different widths of the Gaussian kernel, in which the blurred level describes the Gaussian responses of all points. For each point, we input the point and its ten neighboring points to the Gaussian kernel to calculate the Gaussian response at the point. Finally, the DoG response is obtained by subtracting the two blurred levels

$$\mathcal{F}(x, y, z) = \boldsymbol{G}_1(x, y, z; \sigma_1) - \boldsymbol{G}_2(x, y, z; \sigma_2) \tag{1}$$

where $\mathcal{F}$ is the DoG response of the filtered BLS point cloud and represents the difference between the blurred levels, and $\boldsymbol{G}$ is the 1-D Gaussian response

$$\boldsymbol{G}(x, y, z; \sigma) = \frac{1}{\sqrt{2\pi}\sigma} e^{-\frac{(|(x,y,z)|-\mu)^2}{2\sigma^2}} \tag{2}$$

where the σ represents the width of the Gaussian kernel. In statistics, σ is the SD and σ^2 is the variance. μ is the average of depth and determined by a point and its ten neighboring points. Finally, we detect these points with the local minima or maxima $\mathcal{F}$ value as the point features.

In addition, to extract evenly distributed points, we divide the filter BLS point cloud into multiple subsets according to the aforementioned method of line feature extraction. For each full field-of-view subset, we divide it into six equal parts and then extract the points with the minimum and the maximum $\mathcal{F}$ values (see Fig. 3). Let $\mathcal{R}_n^L$ be the set of point features in the time of sweep n.

C. Scan-to-Scan Matching

The scan-to-scan matching registers two adjacent scans, in which one scan is regarded as the matched scan, and the other is regarded as the reference. In practice, scan-to-scan matching contains two steps: feature matching and rigid transformation estimation. In the feature matching step, the Euclidean nearest neighbor search is adopted to find the corresponding feature pairs, and the distance between the matched features is regarded as the matching constraint.

Line-based registration method has been demonstrated as an effective strategy for point cloud registration [43]. For a tree stem, the trunk skeletons that are derived from the matched scan and the correspondences are similar, but they are not exactly the same because of the sparsity of the BLS data. By contrast, the skeleton nodes maintain a uniform distribution with the corresponding trunk skeleton in its reference, so the point-to-line (skeleton node to line) distance establishes a more accurate relationship between the BLS point clouds. If a trunk skeleton node has two nearest skeleton nodes in the reference data that are within a certain neighborhood of the node, then we set the trunk skeleton node as a keypoint and regard the line that is composed by the two nearest skeleton nodes as a correspondence for transformation estimation. The point-to-line distance d_l can be computed by

$$d_l = \frac{\left|\left(X_{(t+1,l)} - X_{(t,a)}\right) \times \left(X_{(t+1,l)} - X_{(t,b)}\right)\right|}{\left|X_{(t,a)} - X_{(t,b)}\right|} \tag{3}$$

where $X_{(t+1,l)}$ is a trunk skeleton node at the time of sweep, $t+1$, and $X_{(t,a)}$ and $X_{(t,b)}$ are the two nearest skeleton nodes of $X_{(t+1,l)}$ at the time of sweep, t.

In addition, due to fast convergence speed, the planar patch is found to be the correspondence of the point feature. If a point has three nearest points in the reference, and that are within a certain neighborhood and not on the same line, then a planar patch consisting of the three points is regarded as a correspondence of the point feature, and the point will be used as a keypoint for transformation estimation. The point-to-plane distance d_p can be computed by

$$\begin{aligned} d_p &= \frac{\left|\overrightarrow{X_{(t+1,p)}X_{(t,a)}} \cdot \vec{\boldsymbol{n}}\right|}{\left|\vec{\boldsymbol{n}}\right|} \\ &= \frac{\left|\left(X_{(t+1,p)} - X_{(t,a)}\right) \cdot \left(\left(X_{(t+1,p)} - X_{(t,b)}\right) \times \left(X_{(t+1,p)} - X_{(t,c)}\right)\right)\right|}{\left|\left(X_{(t+1,p)} - X_{(t,b)}\right) \times \left(X_{(t+1,p)} - X_{(t,c)}\right)\right|} \end{aligned} \tag{4}$$

where $X_{(t+1,p)}$ is a feature point at the time of sweep, $t+1$, and its corresponding plane at the time of sweep, t, is set to $\left\{X_{(t,a)}, X_{(t,b)}, X_{(t,c)}\right\}$ and $\vec{\boldsymbol{n}}$ is the normal vector of the plane.

Both d_l and d_p tend toward 0. Therefore, the relationship of the corresponding pairs will be more stable and accurate.

When $\boldsymbol{T}$ is the transformation vector between the point cloud and its reference point cloud, the rigid transformation can be represented by six degrees of freedom (6-DOF) and consists of position and attitude during a sweep, i.e.,

$$\boldsymbol{T} = \left[t_x, t_y, t_z, \omega, \varphi, \kappa\right]$$

where t_x, t_y, and t_z are translations along the x-, y-, and z-axes, respectively. ω, φ, and κ are rotation angles around the x-, y-, and z-axes, respectively. Let X_t be the BLS scan at the time of sweep, t, and X_{t+1} be the scan at the time of sweep, $t+1$. Then, a rigid transformation relationship between X_{t+1} and X_t can be established

$$X_t = \boldsymbol{R} X_{t+1} + \boldsymbol{T}(1:3) \tag{5}$$

where $\boldsymbol{R}$ is the rotation matrix ($\boldsymbol{R} \in \mathbb{R}^{3\times 3}$). From (3), we can derive a geometric relationship between each skeleton node in X_{t+1}, and its corresponding line feature in X_t

$$\mathbf{f}_l\left(X_{(t+1,l)}\right) = d_l. \tag{6}$$

Similarly, from (4), we can derive a geometric relationship between a point in X_{t+1} and its correspondence in X_t

$$\mathbf{f}_p\left(X_{(t+1,p)}\right) = d_p. \tag{7}$$

Combining (6) and (7), a nonlinear function in terms of $\boldsymbol{T}$ can be established

$$\mathbf{f}(\boldsymbol{T}) = \sum \mathbf{f}_l\left(X_{(t+1,l)}\right) + \sum \mathbf{f}_p\left(X_{(t+1,p)}\right) \tag{8}$$

where $\mathbf{f}(\cdot)$ represents the distance between the keypoint and its corresponding feature, and each row of $\mathbf{f}$ corresponds to a feature. Finally, (8) can be solved through nonlinear iterations by minimizing the error e toward zero with the Levenberg–Marquardt (L–M) method

$$e = \arg\min_{e} \frac{1}{2} \sum_{i=1}^{N} \|d_i - 0\|^2 = \arg\min \frac{1}{2} \mathbf{f}(\boldsymbol{T})^{\mathrm{T}} \mathbf{f}(\boldsymbol{T}). \tag{9}$$

First, we linearize (9) with the first-order approximation of a Taylor expansion

$$\mathbf{f}(\boldsymbol{T}) = \mathbf{f}\left(\widehat{T} + \Delta \boldsymbol{T}\right) = \mathbf{f}\left(\widehat{T}\right) + \boldsymbol{J} \Delta \boldsymbol{T} \tag{10}$$

where $\widehat{T}$ is the initial transformation in 6-DOF, and $\Delta \boldsymbol{T}$ is the correction of $\widehat{T}$. $\boldsymbol{J}$ is the Jacobian matrix of $\mathbf{f}(\cdot)$. Then, the correction $\Delta \boldsymbol{T}$ can be solved by

$$\Delta \boldsymbol{T} = \left(\boldsymbol{J}^{\mathrm{T}} \boldsymbol{J} + \lambda \boldsymbol{I}\right)^{-1} \boldsymbol{J}^{\mathrm{T}} \boldsymbol{d} \tag{11}$$

where λ is the damping factor, and the scanner motion can be calculated by

$$\boldsymbol{T} = \widehat{T} + \Delta \boldsymbol{T}. \tag{12}$$

Once $\boldsymbol{T}$ is obtained, scan X_{t+1} can be transformed into the coordinate system of scan X_t.

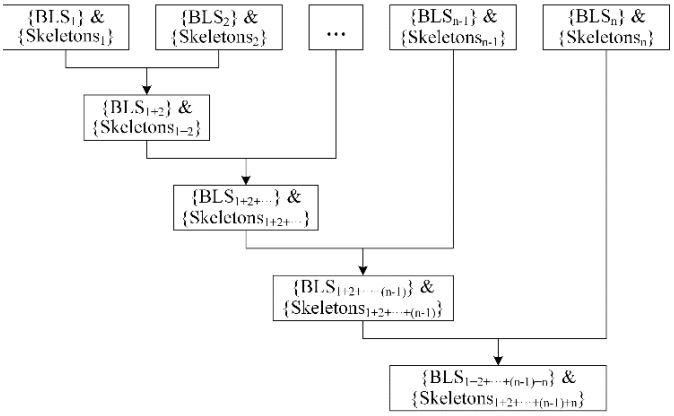

Fig. 4. Schematic of the scan-to-map matching strategy. $\mathrm{BLS}_{(1,2,\ldots,n-1,n)}$ and $\mathrm{Skeletons}_{(1,2,\cdots,n-1,n)}$ represent the BLS scan and its corresponding trunk skeleton nodes at different sweep times, respectively. $\mathrm{BLS}_{(1+2+\cdots n-1+n)}$ and $\mathrm{Skeletons}_{(1+2+\cdots n-1+n)}$ represent the incremental scans and the incremental trunk skeleton nodes, respectively.

D. Scan-to-Map Matching

To maintain mapping accuracy, most of the related methods need to perform numerous loop-closure detections, increasing the algorithm complexity [44]. Compared to the indoor or urban scenes, there are more occlusion effects in forests, but the plot is generally within the range of the LiDAR and has certain permeability. In other words, the objects in the previous BLS scans can still be observed by the subsequent BLS scans. Thus, to mitigate the accumulative error and transform all the BLS point clouds into a common coordinate system, we use the previous BLS scans as constraints and propose a scan-to-map matching strategy for the SLAM process [45], in which the coordinate system of the first frame of the BLS scan is regarded as the common coordinate system, and the defined map consists of the incremental BLS scans and trunk skeleton nodes. The schematic is shown in Fig. 4.

In the strategy, the BLS scan at the time of sweep 1, BLS_1, and its corresponding trunk skeleton nodes, $\mathrm{Skeletons}_1$, are regarded as the reference map, where the BLS scan is used to provide constraint for the point features, and the trunk skeleton nodes are used to provide a constraint for the line features. For the BLS scan at the time of sweep 2, the rigid transformation between BLS_2 and BLS_1 is calculated according to Sections II-B and II-C, and then the current scan and its corresponding skeleton nodes are transformed into the common coordinate system; simultaneously, we rebuild the incremental BLS point clouds BLS_{1+2} and trunk skeleton nodes $\mathrm{Skeletons}_{1+2}$ by combining the data at the time of sweep 1 and 2 and update the two incremental data as a new reference map for optimization. Similarly, for each of the subsequent scans, the transformation at the time of sweep, n, adopts the transformation between the BLS_{n-1} and the reference map as an initial pose, and then, the reference map provides constraints for the rigid transformation estimation; next, the BLS scan and its corresponding skeleton data will be transformed into the common coordinate system and the reference map is updated.

In addition, the mean distance between the skeleton nodes and their corresponding line features is used for determining whether the current BLS point cloud is a keyframe. If the mean distance is less than the set threshold, the current BLS scan will be regarded as a keyframe; furthermore, the BLS scan and its corresponding trunk skeleton nodes are added to the reference map, of which the threshold is an empirical value and set as twice the measurement precision of the scanner.

E. Evaluation Method

The performance of the proposed method is evaluated by the following contents: forest mapping results, mapping accuracy, scan-to-scan matching accuracy, and data performance.

To evaluate the effectiveness of the proposed method, we used the designed BLS system to collect three data sets in forest plots and execute mobile mapping. For evaluation of mapping and scan-to-scan matching accuracy, tree position, branch, and ground position were measured and compared to references, of which the references were collected by using a TLS device through the multiscan method. Specifically, the tree position was used to evaluate the planimetric accuracy, and the branch and ground positions were used to evaluate the vertical accuracy. In addition, due to the limited field of view of the single scanner, the BLS system was limited to acquiring below-canopy information in plots, so DBH was measured to evaluate data performance. In this article, the accuracy was evaluated using the mean distance, root mean square error (RMSE), SD, and the maximum distance, as defined in the following equations:

$$\text{mean} = \frac{\sum_{i=1}^{n} \|x_{Bi} - x_{Ti}\|}{n} \tag{13}$$

$$\text{RMSE} = \sqrt{\frac{\sum_{i=1}^{n} (x_{Bi} - x_{Ti})^2}{n}} \tag{14}$$

$$\text{SD} = \sqrt{\frac{1}{n} \sum_{i=1}^{n} (\|x_{Bi} - x_{Ti}\| - \mu)^2} \tag{15}$$

$$\max = \max(\|x_{Bi} - x_{Ti}\|) \tag{16}$$

where x_{Bi} is the ith measurement, x_{Ti} is the ith reference, and μ is the average. In the evaluation of planimetric accuracy, x_{Bi} is a coordinate component of the tree position in the directions of the x- and y-axes. In the evaluation of vertical accuracy, x_{Bi} is a coordinate component in the direction of the z-axis. In the data performance, x_{Bi} is the DBH measurement. The mean error indicates the mean difference between all measured values and references, RMSE indicates the variability of all errors, and SD indicates the dispersion of all errors.

III. Experimental Results

A. Study Area and Data Acquisition

The study area, located in Saihanba National Forest Park in Hebei Province in northern China, is dominated by coniferous trees. For this study, we acquired three sets of data in different plots of approximately 30 m × 30 m in size. A single scanner BLS system is designed in this study and consists of a single scanner (VELODYNE LiDAR Puck), a portable power source, a data recording device, and a backpack frame (a test system is shown in Fig. 5), where the single laser scanner is mounted horizontally on the backpack frame and approximately 10 cm above the head, and generates up to approximately 400 000 points/s, across a 360° horizontal field of view and a 30° vertical field of view, and the rotation rate was set to 10 Hz in this study, i.e., ten BLS scans are acquired in a second. In addition, a laptop is used to control the scanner and record forest point clouds with the help of the software VeloView. The parameters of the scanner are shown in Table I [46].

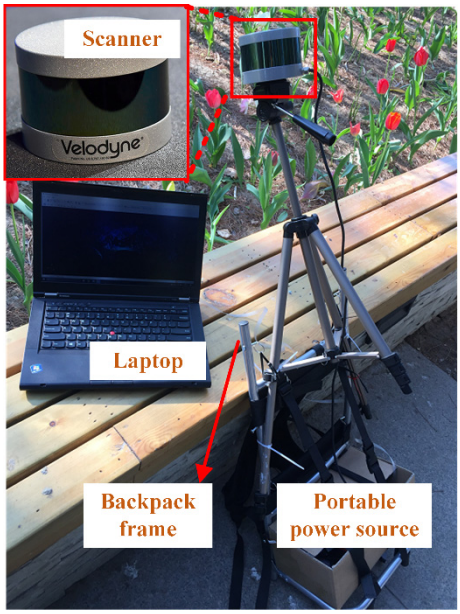

Fig. 5. BLS system, including a single laser scanner, a backpack frame, a portable power source, and a laptop.

TABLE I
Parameters of the BLS System

Scanner	VELODYNE Puck™
Channels	16
Measurement Range	100 m
Range Accuracy	Up to ±3 cm
Field of View (Vertical)	+15.0° to -15.0° (30°)
Angular Resolution (Vertical)	2.0°
Angular Resolution (Horizontal/Azimuth)	0.1° - 0.4°
Rotation Rate	5 Hz – 20 Hz

To evaluate the effectiveness and reliability of the proposed method, three sets of data were collected using the BLS system, which was carried in the test plots at a moving speed of 0.6–0.7 m/s. In the three data sets, 1918, 1395, and 1045 BLS scans were acquired from the forest plots by moving with an s-shape pattern. After collecting forest point clouds based on the BLS system, we immediately used a TLS (RIEGL VZ-1000) device to acquire forest point clouds in each test plot and provide references for algorithm evaluation, and the multi-scan method was applied, i.e., five scans per plot at the center and four-quadrant angles, and the scans were registered with

TABLE II
PLANIMETRIC ACCURACY

Datasets	Number of trees	Planimetric distances (m)			
		Mean	RMSE	SD	Max
1	17	0.023	0.026	0.011	0.051
2	16	0.028	0.030	0.010	0.043
3	16	0.020	0.024	0.013	0.041

the help of artificial reflectors and RIEGL RiSCAN PRO [47]. In addition, the tree positions and DBH values measured from the TLS data were regarded as references for evaluating the accuracy, in which the measurements from TLS data show that the mean DBH varies between 0.2 and 0.4 m in the test forest plots.

B. Forest Plot Mapping

The proposed method is implemented on a computer with an Intel Core i7-3520M CPU at 2.90 GHz. We achieved forest plot mapping and recovered the trajectory of the BLS system (Fig. 6), of which the amount of keyframe BLS scans was a third to a half of the amount of the total scans in each data set, and the runtimes were approximately 30, 25, and 18 min for the test data, i.e., approximately 1 s for each frame BLS point cloud.

Fig. 6 shows that the below-canopy structural information in the test plots is reconstructed by using the BLS system, and the trajectories are coincident with the practical movements. Each tree in the three data sets is registered with no significant deviations, and the distribution of trees is identifiable, which suggests that the individual trees reconstructed by the proposed method have the potential to be applied to forest inventories. In addition, the trajectories of the BLS system do not drift from their correct values in the three data sets, e.g., the trajectory is closed without a loop-closure detection process [in Fig. 6(a)], and the open trajectories in Fig. 6(b) and (c) are still recovered by the proposed method.

C. Mapping Accuracy

To quantitatively evaluate the performance of the proposed method, the tree position measured in the mapping results was compared to that from multiscan TLS data and used to assess the planimetric accuracy of the mapping results. Specifically, each mapping result was manually registered with its corresponding multiscan TLS data; then, 17, 16, and 16 trees were selected from the three data sets and used for calculating tree position distance (Table II).

Table II shows that mean errors, RMSEs, and the maximum errors are at the centimeter level, of which the mean distances and SDs vary between 0.02 and 0.03 m. The SDs are approximately 0.01 m, which indicated a stable distribution. In addition to tree position, the branch points can reflect the vertical accuracy. Therefore, the vertical distances between the branch points in the mapping results and their references in the multiscan TLS data were calculated for evaluating the vertical accuracy (Table III).

Table III shows that the mean distances, RMSEs, and the maximum distances are at the centimeter level, of which

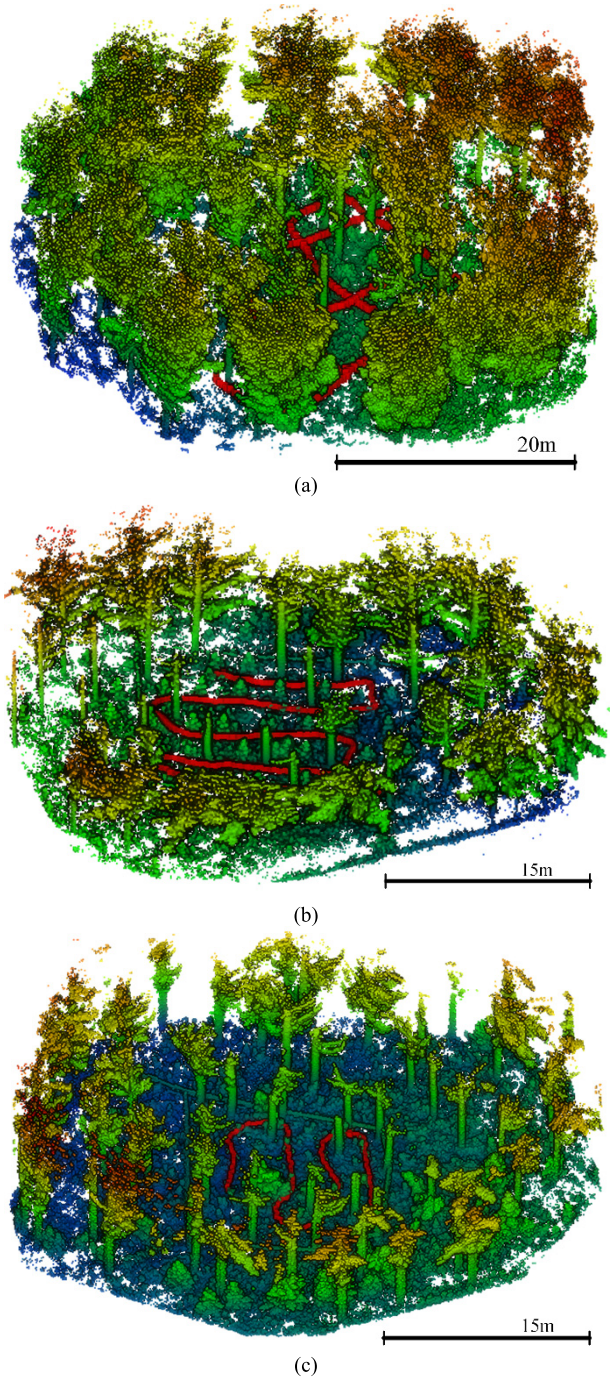

Fig. 6. Forest mapping results. (a)–(c) Mapping results of data sets 1, 2, and 3, respectively, where red curved points represent the moving trajectories of the BLS system in the test plots.

the mean distances and RMSEs are approximately 0.02 m, and the SDs are approximately 0.01 m. In general, high accuracy is required for the registration in the horizontal direction, which needs to meet the requirements of the forest measurements (e.g., DBH), and the requirement of the vertical accuracy is lower than in the horizontal direction (e.g., tree height measurement), so the accuracies indicated effectiveness of the results. In other words, the overall results suggested that the proposed scan-to-map matching strategy can achieve

TABLE III
VERTICAL ACCURACY

Datasets	Number of points	Vertical distances (m)			
		Mean	RMSE	SD	Max
1	20	0.019	0.021	0.011	0.039
2	20	0.016	0.018	0.008	0.030
3	20	0.021	0.023	0.010	0.036

TABLE IV
PLANIMETRIC ERRORS

Datasets	Methods	Number	Planimetric distances (m)			
			Mean	RMSE	SD	Max
1	LOAM	12	0.055	0.061	0.025	0.113
	ICP	12	0.044	0.046	0.013	0.064
	Ours	12	0.015	0.017	0.008	0.033
2	LOAM	12	0.061	0.069	0.031	0.126
	ICP	12	0.035	0.036	0.010	0.058
	Ours	12	0.015	0.017	0.008	0.029
3	LOAM	12	0.052	0.055	0.018	0.086
	ICP	12	0.051	0.053	0.016	0.072
	Ours	12	0.018	0.019	0.006	0.028

BLS-based forest plot mapping, of which the map provides effective consistency constraints for each BLS point cloud.

IV. DISCUSSION

A. Comparison of Scan-to-Scan Matching

In this article, line and point features were used to solve the planimetric and vertical errors of registration in the forest plots, respectively. To evaluate the effectiveness of the features in scan-to-scan matching, we analyzed two frames of BLS point cloud registration results according to the trees and ground position and compared the proposed method with two methods: the ICP and LOAM methods. For the planimetric accuracy, some trees were selected from the three data sets, to calculate the tree position distances. We projected the stem points that are above the ground to a plane and estimated the centers of the circles by the least squares method. Then, the centers were regarded as tree positions, and the distances between the tree positions in the registered scan and the corresponding positions in the reference scan were calculated. The tree position distances are summarized in Table IV.

The results from the LOAM and ICP methods show greater distances than those of the proposed method, especially the LOAM method. The mean distances and RMSEs calculated by the LOAM methods vary between 0.05 and 0.07 m for the three data sets, and the maximum distance is approximately 0.1 m. The mean distances and RMSEs of the ICP method vary between 0.03 and 0.06 m. In contrast, the proposed method performs well, of which the mean distances and RMSEs are less than 0.02 m in the three data sets, the SDs are at the millimeter level, and the maximum distances are approximately 0.03 m. The LOAM method matches scans, combining the line and plane features, and requires a fine initial transformation. Without an initial transformation for the LOAM method, the reliable features are difficult to extract directly from the forest, and inaccurate corresponding pairs in adjacent scans cause the LOAM method to fall into local minima and result in large planimetric errors. In addition, the ICP method was used to estimate the transformation between scans, which considers all points in the registration and requires high overlap of point clouds. Although the BLS scans were acquired in adjacent locations, there are certain errors in the matching of the two adjacent BLS scans because of the sparsity of the BLS scan. In contrast, the proposed line features are stable and provide a strong constraint for scan-to-scan matching in the horizontal direction, so the proposed method obtained smaller tree position errors.

TABLE V
VERTICAL ERRORS

Datasets	Methods	Number	Vertical distances (m)			
			Mean	RMSE	SD	Max
1	LOAM	20	0.007	0.008	0.003	0.016
	ICP	20	0.058	0.077	0.024	0.115
	Ours	20	0.009	0.010	0.005	0.023
2	LOAM	20	0.009	0.011	0.006	0.023
	ICP	20	0.048	0.083	0.028	0.106
	Ours	20	0.007	0.009	0.005	0.025
3	LOAM	20	0.010	0.012	0.006	0.021
	ICP	20	0.041	0.047	0.025	0.112
	Ours	20	0.008	0.009	0.005	0.018

In addition to the planimetric accuracy, we also analyzed the vertical error based on the branch position distance. In the three data sets, some points on the ground were selected to verify the proposed method. We then calculated the distance between the points in the registered point cloud and their correspondences in the reference scan (Table V).

The vertical distances from the LOAM method and the proposed method show approximate performance, in which the mean distances and RMSEs are approximately 0.01 m in the three data sets, and the SDs are at the millimeter level, which indicates highly accurate scan-to-scan matching. In contrast, the results of the ICP method show large distances, of which the mean distances and RMSEs are greater than 0.04 m and the maximum deviations are greater than 0.1 m in the three data sets. The LOAM method and the proposed method extracted some uniform distributed features in the forest plots, including some points of ground and branches. Due to strong constraints from the ground and branches, the LOAM method and the proposed method perform well in the vertical direction. However, due to the specific attributes of the scanner, the BLS scan is sparse in the vertical direction, and there is low overlap between the point clouds acquired from different perspectives. Consequently, sparse ground and branch points encounter difficulty providing effective constraints for scan matching based on the ICP method.

The results in Tables IV and V show that the major difference between the LOAM method and the proposed method is shown in the planimetric deviations. The proposed method estimates the rigid transformation between the BLS scans without an initial transformation, in which the trunk skeleton lines can provide accurate corresponding pairs and effectively solve the problem of inaccurate registration in the horizontal direction and then ensure the planimetric accuracy of forest mapping; meanwhile, the point-to-plane correspondence provides an effective constraint for matching in the vertical direction.

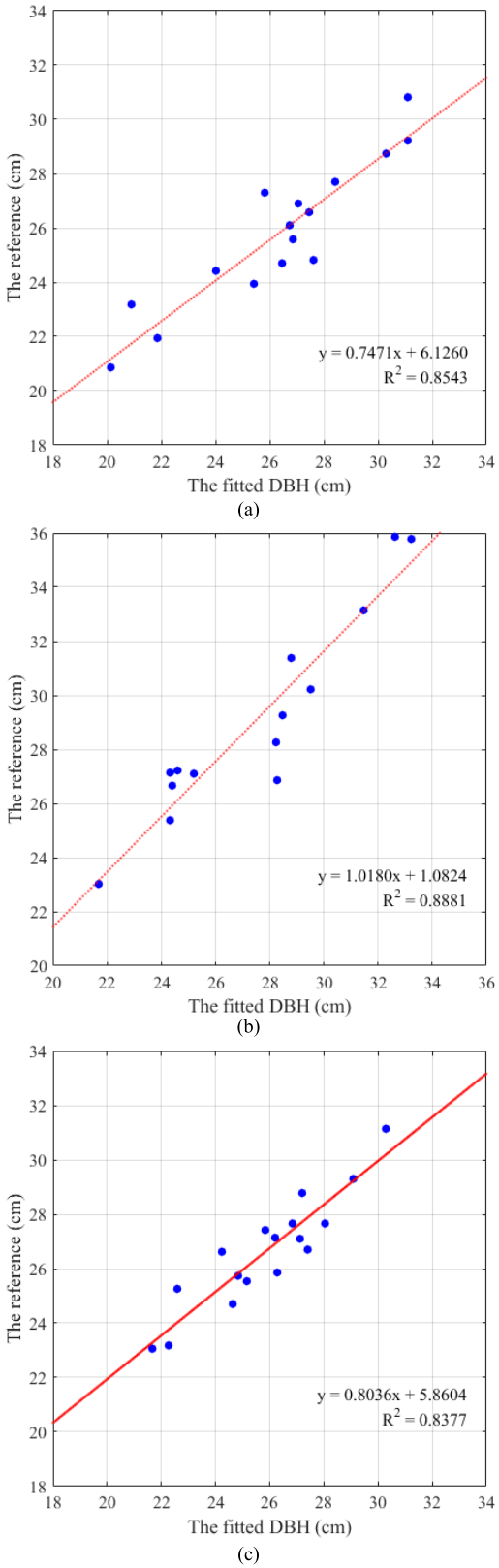

Fig. 7. Scatterplots of the DBH values. The y-axis represents the reference of DBH values from the multiscan TLS point cloud and the x-axis represents the fit DBH from the results of the proposed method. (a)–(c) Data sets 1, 2, and 3, respectively.

B. Data Performance

The test BLS system integrated a single scanner, which was placed horizontally so that below-canopy data were scanned, but the canopy and above-canopy information were limited by the vertical field of view of the scanner. Therefore, to analyze applications of the mapping results in forest measurements, we selected an important forest parameter, DBH, to evaluate the effectiveness of the mapping results. We calculated the DBH values in the test plots and compared with those from the multi-scan TLS data. The DBH of individual trees is determined by extracting a cross-section of the point cloud that falls between 1.2 and 1.4 m above the ground level. First, we filtered the ground and nonground points [48] and extracted points that represented the tree stem hull at the breast height from the nonground points and then used the least square method to fit a circle. The accuracy of the DBH values is assessed by treating the reference as a variable that is dependent upon the fit measurement and running a simple linear regression analysis to determine the coefficient of determination (R^2) for the three data sets (Fig. 7).

The results of the linear regression analysis revealed that the coefficient of determination between the fit DBH, measured from the data via the proposed method and the fit DBH from the multiscan TLS data, is greater than 0.8 in the test plots, which indicated a significant correlation between the DBH measured from the proposed method and the multi-scan TLS data. In data set 1, the RMSE is 1.4 cm and the mean absolute error (MAE) is 1.2 cm, of which the total error is approximately 95%. In data set 2, the RMSE between the fit DBH values and the measured DBH values from TLS data is 2 cm and the MAE is 1.8 cm, and the total error is approximately 94%. In data set 3, the MAE is 1 cm and the RMSE is 1.2 cm, and the total error is approximately 96%. Overall, the total errors are more than 90% in the test plots, which indicated reliable mapping results. Therefore, the results suggested the effectiveness of the proposed line features and optimization strategy for maintaining the planimetric accuracy of the forest plot mapping.

V. Conclusion

LiDAR-based mapping has been one of the most important developments for forest measurements. To achieve fast forest point cloud acquisition, this article designed a single scanner BLS system and proposed a new mapping method. The system is simple and specific to forest plots. Subsequently, practical experiments were implemented to evaluate the effectiveness and reliability of the BLS system and the proposed method. In practice, the BLS system took only a few minutes to scan a forest plot, and its efficiency is higher than that of the multiscan TLS method. To achieve accurate matching, the line features derived from the tree trunk skeletons were proposed and used to calculate the rigid transformation, and the line feature solved the inaccurate registration problem caused by insufficient point cloud overlap and inaccurate corresponding pairs in the horizontal direction. Compared to the existing methods, the scan matching results from the proposed method were more accurate. In addition, the optimization framework based on the scan-to-map matching strategy is used to provide consistency constraints for the BLS-based SLAM in the forest environments and ensure mapping accuracies without a loop-closure detection process, in which the map consists of the

incremental BLS point clouds and the tree trunk skeleton nodes, and the incremental trunk skeleton nodes maintained accurate registration of all individual trees, especially tree stems.

The proposed method achieved fast data acquisition in forest plots, but the data acquired by a single scanner were limited to below-canopy. In the future, therefore, to acquire higher forest layer, two scanners will be considered, of which one is placed horizontally for the SLAM method and below-canopy data acquisition and the other vertically for acquiring information in the higher forest layer. In addition, point cloud distortion caused by motion blur also affects the measurement precision and data quality, which can lead to inaccurate matching results. Therefore, we still need to consider reducing the distortion and improve point cloud quality.

REFERENCES

[1] X. Liang *et al.*, "Terrestrial laser scanning in forest inventories," *ISPRS J. Photogramm. Remote Sens.*, vol. 115, pp. 63–77, May 2016.

[2] J. Hyyppä, "Feasibility for estimation of single tree characteristics using laser scanner," *Int. Geosci. Remote Sens. Symp.*, vol. 3, Jul. 2000, pp. 981–983.

[3] G. E. Murphy, M. A. Acuna, and I. Dumbrell, "Tree value and log product yield determination in radiata pine (Pinus radiata) plantations in Australia: Comparisons of terrestrial laser scanning with a forest inventory system and manual measurements," *Can. J. Forest Res.*, vol. 40, no. 11, pp. 2223–2233, Nov. 2010.

[4] L. Luo *et al.*, "Airborne and spaceborne remote sensing for archaeological and cultural heritage applications: A review of the century (1907–2017)," *Remote Sens. Environ.*, vol. 232, Oct. 2019, Art. no. 111280.

[5] H. Latifi, F. E. Fassnacht, J. Müller, A. Tharani, S. Dech, and M. Heurich, "Forest inventories by LiDAR data: A comparison of single tree segmentation and metric-based methods for inventories of a heterogeneous temperate forest," *Int. J. Appl. Earth Observ. Geoinf.*, vol. 42, pp. 162–174, Oct. 2015.

[6] P. Wilkes *et al.*, "Data acquisition considerations for terrestrial laser scanning of forest plots," *Remote Sens. Environ.*, vol. 196, pp. 140–153, Jul. 2017.

[7] G. J. Newnham *et al.*, "Terrestrial laser scanning for plot-scale forest measurement," *Current Forestry Rep.*, vol. 1, no. 4, pp. 239–251, Dec. 2015.

[8] S. Bauwens, H. Bartholomeus, K. Calders, and P. Lejeune, "Forest inventory with terrestrial LiDAR: A comparison of static and hand-held mobile laser scanning," *Forests*, vol. 7, no. 12, p. 127, Jun. 2016.

[9] J. L. Lovell, V. Haverd, D. L. B. Jupp, and G. J. Newnham, "The canopy semi-analytic Pgap and radiative transfer (CanSPART) model: Validation using ground based lidar," *Agricult. Forest Meteorol.*, vols. 158–159, pp. 1–12, Jun. 2012.

[10] W. Zhang, Y. Chen, H. Wang, M. Chen, X. Wang, and G. Yan, "Efficient registration of terrestrial LiDAR scans using a coarse-to-fine strategy for forestry applications," *Agricult. Forest Meteorol.*, vol. 225, pp. 8–23, Sep. 2016.

[11] A. Kukko, H. Kaartinen, J. Hyyppä, and Y. Chen, "Multiplatform mobile laser scanning: Usability and performance," *Sensors*, vol. 12, no. 9, pp. 11712–11733, Aug. 2012.

[12] X. Liang, J. Hyyppa, A. Kukko, H. Kaartinen, A. Jaakkola, and X. Yu, "The use of a mobile laser scanning system for mapping large forest plots," *IEEE Geosci. Remote Sens. Lett.*, vol. 11, no. 9, pp. 1504–1508, Sep. 2014.

[13] M. Miettinen, M. Ohman, A. Visala, and P. Forsman, "Simultaneous localization and mapping for forest harvesters," in *Proc. IEEE Int. Conf. Robot. Autom.*, Apr. 2007, pp. 517–522.

[14] M. Holopainen *et al.*, "Tree mapping using airborne, terrestrial and mobile laser scanning—A case study in a heterogeneous urban forest," *Urban Forestry Urban Greening*, vol. 12, no. 4, pp. 546–553, Jan. 2013.

[15] L. Chang, X. Niu, T. Liu, J. Tang, and C. Qian, "GNSS/INS/LiDAR-SLAM integrated navigation system based on graph optimization," *Remote Sens.*, vol. 11, no. 9, p. 1009, Apr. 2019.

[16] J. Tang *et al.*, "SLAM-aided stem mapping for forest inventory with small-footprint mobile LiDAR," *Forests*, vol. 6, no. 12, pp. 4588–4606, Dec. 2015.

[17] M. W. M. G. Dissanayake, P. Newman, S. Clark, H. F. Durrant-Whyte, and M. Csorba, "A solution to the simultaneous localization and map building (SLAM) problem," *IEEE Trans. Robot. Autom.*, vol. 17, no. 3, pp. 229–241, Jun. 2001.

[18] M. Pierzchała, P. Giguère, and R. Astrup, "Mapping forests using an unmanned ground vehicle with 3D LiDAR and graph-SLAM," *Comput. Electron. Agricult.*, vol. 145, pp. 217–225, Feb. 2018.

[19] A. J. Davison, I. D. Reid, N. D. Molton, and O. Stasse, "MonoSLAM: Real-time single camera SLAM," *IEEE Trans. Pattern Anal. Mach. Intell.*, vol. 29, no. 6, pp. 1052–1067, Jun. 2007.

[20] J. Engel, T. Schöps, and D. Cremers, "LSD-SLAM: Large-scale direct monocular SLAM," in *Proc. Eur. Conf. Comput. Vis.*, 2014, pp. 834–849.

[21] C. Forster, M. Pizzoli, and D. Scaramuzza, "SVO: Fast semi-direct monocular visual odometry," in *Proc. IEEE Int. Conf. Robot. Autom. (ICRA)*, May 2014, pp. 15–22.

[22] R. Mur-Artal, J. M. M. Montiel, and J. D. Tardos, "ORB-SLAM: A versatile and accurate monocular SLAM system," *IEEE Trans. Robot.*, vol. 31, no. 5, pp. 1147–1163, Oct. 2015.

[23] S. Kohlbrecher, O. von Stryk, J. Meyer, and U. Klingauf, "A flexible and scalable SLAM system with full 3D motion estimation," in *Proc. IEEE Int. Symp. Saf., Secur., Rescue Robot.*, Nov. 2011, pp. 155–160.

[24] G. Grisetti, C. Stachniss, and W. Burgard, "Improved techniques for grid mapping with Rao-Blackwellized particle filters," *IEEE Trans. Robot.*, vol. 23, no. 1, pp. 34–46, Feb. 2007.

[25] K. Konolige, G. Grisetti, R. Kümmerle, W. Burgard, B. Limketkai, and R. Vincent, "Efficient sparse pose adjustment for 2D mapping," in *Proc. IEEE/RSJ Int. Conf. Intell. Robots Syst.*, Oct. 2010, pp. 22–29.

[26] W. Hess, D. Kohler, H. Rapp, and D. Andor, "Real-time loop closure in 2D LIDAR SLAM," in *Proc. IEEE Int. Conf. Robot. Autom. (ICRA)*, May 2016, pp. 1271–1278.

[27] J. M. Santos, D. Portugal, and R. P. Rocha, "An evaluation of 2D SLAM techniques available in robot operating system," in *Proc. IEEE Int. Symp. Saf., Secur., Rescue Robot. (SSRR)*, Oct. 2013, pp. 1–6.

[28] J. Zhang and S. Singh, "LOAM: Lidar odometry and mapping in real-time," *Robot., Sci. Syst.*, vol. 2, no. 9, pp. 1–9, Jul. 2014.

[29] J.-E. Deschaud, "IMLS-SLAM: Scan-to-model matching based on 3D data," in *Proc. IEEE Int. Conf. Robot. Autom. (ICRA)*, May 2018, pp. 2480–2485.

[30] C. Qian *et al.*, "An integrated GNSS/INS/LiDAR-SLAM positioning method for highly accurate forest stem mapping," *Remote Sens.*, vol. 9, no. 1, p. 3, Dec. 2016.

[31] R. Cifuentes, D. Van der Zande, J. Farifteh, C. Salas, and P. Coppin, "Effects of voxel size and sampling setup on the estimation of forest canopy gap fraction from terrestrial laser scanning data," *Agricult. Forest Meteorol.*, vol. 194, pp. 230–240, Aug. 2014.

[32] D. Kelbe, J. van Aardt, P. Romanczyk, M. van Leeuwen, and K. Cawse-Nicholson, "Marker-free registration of forest terrestrial laser scanner data pairs with embedded confidence metrics," *IEEE Trans. Geosci. Remote Sens.*, vol. 54, no. 7, pp. 4314–4330, Jul. 2016.

[33] Y. Chen *et al.*, "Scan matching technology for forest navigation with map information," in *Proc. IEEE/ION Position, Location Navigat. Symp. (PLANS)*, Apr. 2016, pp. 198–203.

[34] A. Kukko, R. Kaijaluoto, H. Kaartinen, V. V. Lehtola, A. Jaakkola, and J. Hyyppä, "Graph SLAM correction for single scanner MLS forest data under boreal forest canopy," *ISPRS J. Photogramm. Remote Sens.*, vol. 132, pp. 199–209, Oct. 2017.

[35] J. Liu *et al.*, "Automated matching of multiple terrestrial laser scans for stem mapping without the use of artificial references," *Int. J. Appl. Earth Observ. Geoinf.*, vol. 56, pp. 13–23, Apr. 2017.

[36] P. Polewski, W. Yao, L. Cao, and S. Gao, "Marker-free coregistration of UAV and backpack LiDAR point clouds in forested areas," *ISPRS J. Photogramm. Remote Sens.*, vol. 147, pp. 307–318, Jan. 2019.

[37] P. J. Besl and N. D. McKay, "A method for registration of 3-D shapes," *IEEE Trans. Pattern Anal. Mach. Intell.*, vol. 14, no. 2, pp. 239–256, Feb. 1992.

[38] W. Zhang *et al.*, "A novel approach for the detection of standing tree stems from plot-level terrestrial laser scanning data," *Remote Sens.*, vol. 11, no. 2, p. 211, Jan. 2019.

[39] N. Mellado *et al.* Patate: A C++ library provides tools to represent, characterize and analyze data commonly used in computer graphics, version 2.0. library: PATATE. [Online]. Available: https://gitlab.inria.fr/patate/patate

[40] R. Gonzalez and R. Woods, *Digital Image Processing*. New York, NY, USA: Pearson, 2018.
[41] P. W. Theiler, J. D. Wegner, and K. Schindler, "Keypoint-based 4-points congruent sets—Automated marker-less registration of laser scans," *ISPRS J. Photogramm. Remote Sens.*, vol. 96, pp. 149–163, Oct. 2014.
[42] R. B. Rusu and S. Cousins, "3D is here: Point cloud library (PCL)," in *Proc. IEEE Int. Conf. Robot. Autom.*, May 2011, pp. 1–4.
[43] P. Polewski and W. Yao, "Scale invariant line-based co-registration of multimodal aerial data using l1 minimization of spatial and angular deviations," *ISPRS J. Photogramm. Remote Sens.*, vol. 152, pp. 79–93, Jun. 2019.
[44] J. Shao *et al.*, "Automated markerless registration of point clouds from TLS and structured light scanner for heritage documentation," *J. Cultural Heritage*, vol. 35, pp. 16–24, Jan. 2019.
[45] J. Shao *et al.*, "SLAM-aided forest plot mapping combining terrestrial and mobile laser scanning," *ISPRS J. Photogramm. Remote Sens.*, vol. 163, pp. 214–230, May 2020.
[46] *Velodyne LiDAR PuckTM*. Accessed: Mar. 24, 2020. [Online]. Available: https://velodynelidar.com/products/puck/
[47] K. Calders, J. Armston, G. Newnham, M. Herold, and N. Goodwin, "Implications of sensor configuration and topography on vertical plant profiles derived from terrestrial LiDAR," *Agricult. Forest Meteorol.*, vol. 194, pp. 104–117, Aug. 2014.
[48] W. Zhang *et al.*, "An easy-to-use airborne LiDAR data filtering method based on cloth simulation," *Remote Sens.*, vol. 8, no. 6, p. 501, Jun. 2016.

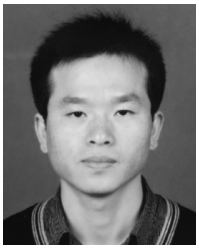

Jie Shao received the B.S. degree in geographic information system from Anhui Normal University, Wuhu, China, in 2010. He is pursuing the Ph.D. degree in cartography and geographic information system with Beijing Normal University, Beijing, China.

He is a Joint Ph.D. Student with the IRIT, CNRS, University of Toulouse, Toulouse, France. His research interests include multisource remote sensing data fusion and light detection and ranging (LiDAR) point cloud processing and applications.

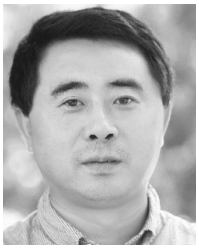

Wuming Zhang received the Ph.D. degree from Tsinghua University, Beijing, China, in 2004.

He is a Professor with the School of Geospatial Engineering and Science, Sun Yat-sen University, Zhuhai, China. His research interests include photogrammetry and remote sensing, especially light detection and ranging (LiDAR) point cloud processing and applications.

Nicolas Mellado received the Ph.D. degree from the Institut National de Recherche en Informatique et en Automatique (INRIA) Bordeaux Sud-Ouest, Bordeaux, France, in 2012.

He is a Researcher with the Institut de Recherche en Informatique de Toulouse (IRIT), CNRS, Université Toulouse III Paul Sabatier, Toulouse, France. His research interests focus on the robust analysis of unstructured point cloud.

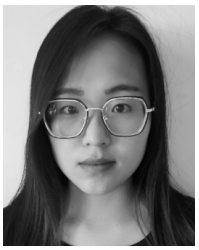

Shuangna Jin received the B.S. degree in surveying and mapping engineering from the Hefei University of Technology, Hefei, China, in 2018. She is pursuing the master's degree in photogrammetry and remote sensing with Beijing Normal University, Beijing, China.

Her research interests include light detection and ranging (LiDAR) point cloud processing and vegetation parameter retrieval.

Shangshu Cai received the B.S. degree in surveying and mapping engineering from Inner Mongolia Agricultural University, Hohhot, China, in 2014. He is pursuing the Ph.D. degree in cartography and geographic information system with Beijing Normal University, Beijing, China.

His research interests focus on light detection and ranging (LiDAR)-based forest inventory.

Lei Luo received the Ph.D. degree in cartography and geographic information system from the University of Chinese Academy of Sciences, Beijing, China, in 2016.

He is an Assistant Professor with the Aerospace Information Research Institute, Chinese Academy of Sciences, Beijing. His research interests include multiplatform Earth observation technologies, big Earth data for archaeological prospecting, and cultural and natural heritage conservation.

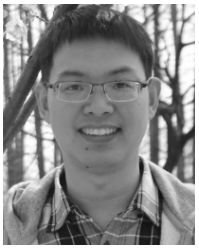

Lingbo Yang received the B.S. degree in geographic information system from the Hefei University of Technology, Hefei, China, in 2010. He is pursuing the Ph.D. degree with Zhejiang University, Hangzhou, China.

He was employed by the Food and Agriculture Organization of the United Nations (FAO) as a Geospatial Specialist in 2019. His research interests include geographic information system, remote sensing, and machine learning, especially in agricultural and forestry remote sensing.

Guangjian Yan (Senior Member, IEEE) received the Ph.D. degree from the Institute of Remote Sensing Applications, Chinese Academy of Sciences, Beijing, China, in 1999.

He is a Professor with the State Key Laboratory of Remote Sensing Science, Faculty of Geographical Science, Beijing Normal University, Beijing. He has authored over 200 articles. His research interests include multiangular remote sensing, vegetation remote sensing, and radiation budget.

Guoqing Zhou received the Ph.D. degree from Wuhan University, Wuhan, China, in 1994.

He is a Professor with the Guangxi Key Laboratory for Spatial Information and Geomatics, Guilin University of Technology, Guilin, China. His research interests include photogrammetry and remote sensing, especially in remote sensing image processing and interpretation.